ELSEVIER

Journal of Nuclear Materials 273 (1999) 285–293

journal of nuclear materials

www.elsevier.nl/locate/jnucmat

Intrinsic hydrogen transport constants in the CFC matrix and fibres derived from isovolumetric desorption experiments

Luis A. Sedano *, Adolfo Perujo, Chung H. Wu

European Commission, JRC-Ispra, E.I., Hydrogen Materials Interact. Sect., 21020 Ispra VA, Italy
The NET Team, Max-Planck-Institut für Plasmaphysik, D-85748 Garching, Germany

Received 11 December 1998; accepted 15 February 1999

Abstract

The manufacture of carbon fibre composites (CFC) requires models differentiating the transport mechanisms in the CFC fibres and in the matrix. A non-stationary model was developed for isovolumetric desorption experiments (IDE) and checked with results for a well-characterised homogeneous material (Ni). The apparent transport constants for three CFC (N112, NS31 and N11) from Société Européenne de Propulsion (SEP), were derived. However, the fitting of the experimental hydrogen release using the homogeneous model is unsatisfactory, in that the experimental curve shows two overlapping time constants. The analysis of the hydrogen paths served to build a non-homogeneous diffusive model that fits accurately the experimental release. The intrinsic values of the fibre and the matrix derived for the three CFC studied are comparable. Values for the hydrogen diffusivity in the matrix are 6–7 orders of magnitude higher than in the fibres. The determinant role of fibres on the hydrogen solubility in the studied CFC is shown.

Notation

H	Hydrogen
D	Hydrogen diffusivity
K_s	Sieverts' constant
CFC	Carbon fibre composites
c_1	Sample distribution during loading
c_2	Sample distribution during pumping
c_3	Sample distribution during the release
p_L	Loading pressure
c_L	Equilibrium concentration during loading
$c_{\Delta t}$	Equilibrium concentration: end of the pumping phase
c_f	Equilibrium concentration: end of the release phase
t	Time
Δt	Duration of pumping phase
r	Radial co-ordinate at the cylindrical case
x	Linear co-ordinate
β	Fitting parameter
γ	Fitting parameter
α_n	Root of $J_0(a\ \alpha_n)=0$
τ	Loading time
τ^*	Loading time for saturation
T	Temperature
J_T	Total flux of H atoms
$p(t)$	Pressure in V_1
a	Cylinder radii
Δx	Thickness of the plate
R	Gas perfect constant
V_1	Chamber volume
V_s	Volume of a sample
N_A	Avogadro's number
D_M	Hydrogen diffusivity in the matrix
D_F	Hydrogen diffusivity in fibres
D_{FM}	In series hydrogen effective diffusivity for fibre and matrix
E_d	Diffusion energy
E_s	Solution energy

* Corresponding author. Tel.: +39 0332 785321; fax: +39 0332 785029; e-mail: luis.sedano@jrc.it

0022-3115/99/$ – see front matter
PII: S0022-3115(99)00055-0

1. Introduction

The determination of the carbon fibre composites' (CFC) hydrogen (H) transport constants, diffusivity (D) and Sieverts constant (K_s), is of great interest in several fields of composite science and industrial technology. The design of CFC components for hydrogen propulsion space engines and the tracking of hydrogen isotopes in CFC-made plasma facing components of fusion reactors are examples.

Anisotropy has been commonly proposed to explain the large scattering (sometimes several orders of magnitude) found in literature for hydrogen transport constants in graphite. At 1073 K, the diffusivity can range from 10^{-12} m^2/s, for A3 [1] to 10^{-22} m^2/s for YPD [2] and K_s can range from 8×10^{-7} at.fr.Pa$^{-1/2}$(IG-430U) [2] to 6×10^{-6} at.fr.Pa$^{-1/2}$ (IG-110U) [3]. Hence, the extrapolation of further applications of hydrogen transport data of graphite to carbon composites appears quite inappropriate.

Isovolumetric desorption experiment (IDE) is a classical measuring technique used to determine the hydrogen transport parameters (D and K_s) in materials. The experimental procedure starts with the loading of the sample with a fixed hydrogen gas pressure, optionally achieving hydrogen saturation in the sample, and to force ultra high vacuum (UHV) conditions in the measuring chamber by fast pumping in order to cause the hydrogen release from the material.

The low hydrogen diffusivity in carbon makes loading and release times for CFC very long (some months) in comparison with metals (18 h for Ni), see Section 2. Thus, the stability of long measurements appears not to be guaranteed.

A non-stationary model has been developed in order to derive D and K_s, when the material is not loaded to saturation, from the fitting of a release curve for measuring times shorter than that needed to achieve the hydrogen steady state release. The detailed characteristics of this homogeneous and non-stationary model and its validation using Ni release data are presented in Section 3.

The homogeneous model was used to derive the *apparent* hydrogen transport constants for three different CFC: N112, N11 and NS31 Société Européenne de Propulsion (SEP), but it is not able to satisfactorily fit the experimental hydrogen release curves from them (Section 4).

The direct analysis of the experimental hydrogen release curves from the composites shows two overlapping processes. The correspondence between the time constants and the hydrogen loading release paths in the CFC served as a basis to develop a non-homogeneous refinement of the previous model. The application of this refined model enabled a complete fitting of the release curve, so obtaining D and K_s for hydrogen separated for both the fibres and matrix (Section 5). Evaluations of the IDE data using this model show the determinant role of the fibres on the total K_s of hydrogen in CFC and the role of the porosity on the diffusivity and Sieverts constant of hydrogen in the matrix. The model capabilities suggest the use for the manufacture of CFC from its hydrogen interaction characteristics stand point.

2. Experimental

An IDE consists of three phases: loading, pumping and release.

During the loading phase (duration: τ), the sample material is charged with hydrogen at a constant pressure of 10^5 Pa. Following the loading duration, an UHV ($\simeq 10^{-7}$ Pa) was established in the measuring chamber V_1 by fast pumping (30 s, pumping phase) of V_1, in order to break the equilibrium (or quasi-equilibrium) state of hydrogen in the sample. The final phase is the observation of the transient release of hydrogen from the material, by measuring the pressure increase in V_1 (release phase), see Fig. 1.

One of the primary difficulties of IDE is the choice for the duration (τ) of the loading phase. The τ values are tentatively fixed on the basis of the time needed to load the sample at saturation (τ^*), which is interrelated to the hydrogen diffusivity in the materials (one of the transport constants to be obtained). Preliminary measurements are usually needed in order to estimate τ^*. Sometimes the τ^* values are estimated on the basis of the hydrogen diffusivity of similar materials to those studied. However, the large scattering of data for graphite makes this approximation doubtful for CFCs.

During the release phase the data acquisition system registers the absolute pressure measured by a capacitance manometer (full range 1 mbar) in V_1 the absolute elapsed time since the release time started, and the temperature. Measurements are performed under isothermal (fluctuation of ±4 K for the maximum temperature of 1200 K) and isovolumetric (i.e. V_1 constant) conditions.

The recording frequency of the measured data is conveniently distributed throughout the release time. It

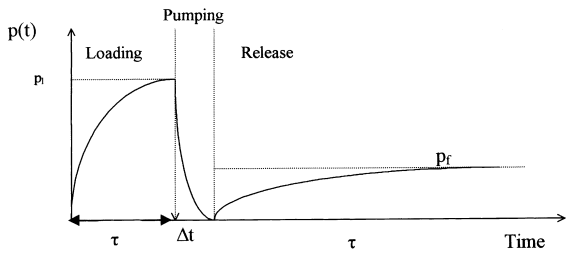

Fig. 1. The three phases in IDE.

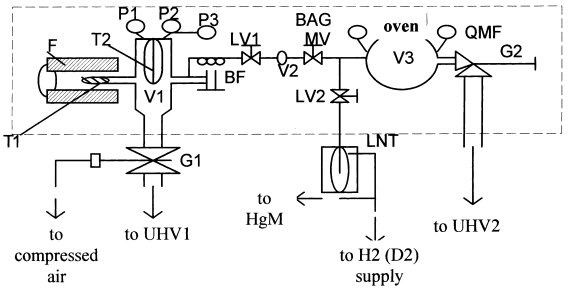

Fig. 2. The general layout of the IDE facility and main units. F: Furnace; V_1: Release Chamber; BAG: Bayarg–Alpert Gauge; G_1, G_2: Gate Valves; HgM: U-tube Hg. Manometer; LV: Leak Value; MV: Manual Valve; P: Capacitance manometer; T_1, T_2: Pt-thermocouple; UHV: Pumping Units; V_2, V_3: Expansion volumes; P_1, P_2, P_3: Pressure measuring heads; QMF: Quadrupole Mass Filter.

is higher during the initial phase of the experiment, where the variation of the pressure in V_1 is most important.

A background release signal was observed originating from the release of hydrogen previously adsorbed during the loading phase at the walls of V_1. Then, a background subtraction was applied to each hydrogen release curve in which the pressure rise of a control experiment (without samples at the same temperature) was subtracted from the experimental release curve. The resulting pressure curve in V_1 is the input curve retained for modelling. The general layout of the IDE facility with its main components is shown schematically in Fig. 2 and presented in more detail in Ref. [4].

To validate the transient model, preliminary measurements of four identical nickel cylinders: (6 mm radius, 60 mm length) and one nickel plate ($10 \times 10 \times 1$ mm^3) were performed in separate experiments. Four CFC cylindrical samples (6 mm radius, 60 mm length) of N112 and N11, and one plate of NS31 ($10 \times 10 \times 1$ mm^3), all from SEP, were studied. The fibres for the three CFC studied exhibit a planar arrangement net of fibres pre-form, with needling (case of N112 and N11) or with pitch fibres (case of NS31), in the orthogonal direction. Exact compositions, matrix porosity, fibre/matrix volume ratio, fibre radius and compositions are detailed in [5]. Virgin samples, as provided by the manufacturer, were outgassed during approx. 10 h at 100°C before the use in the measurements.

3. Modelling IDE

Our main modelling objectives for IDE were:

(1) *The validity of the developed model for any loading time* (τ). As data points are conveniently distributed throughout the experimental measurement, there should not be a statistical constraint when using shorter loading and release times. This aim is important in order to have model predictions for $\tau \ll \tau^*$, even for: $\tau \leqslant \tau^*/20$. After its validation this goal will mean the potential reduction in the measuring times to obtain the same values for D and K_s which are derived from loading/releasing samples up to saturation ($\tau = \tau^*$).

(2) *The precision accounting of the gas balance at the pumping phase*. The amount of gas released from the test specimen during the pumping phase ($\Delta t = 30$ s) is usually small in comparison with the total amount loaded during τ^*. However, it may become significant when using short gas loading times τ (when $\tau \ll \tau^*$) and/or the gas release for times $t \ll \tau^*$. Model precision and success in the previous purpose (1) depend on the accurate gas accounting during the pumping phase.

(3) Finally, the evolution of the sample surface in equilibrium with the surrounding atmosphere of the gas previously released in V_1 has to be considered. Mathematically it implies the inclusion of time dependent boundary condition.

3.1. General case: homogeneous materials

The model solves the diffusion equation without sources for a given geometry (cylinder or plate), while linking the three phases. Starting from an initial zero concentration in the sample, the concentration distribution in the sample after the loading time τ is obtained by solving the diffusion equation and this provides the initial concentration for the pumping phase. The solution of the diffusion equation for the pumping phase is used as the initial condition for the diffusion problem during the release phase.

One original aspect of our model, presented in point (3), is based on the open consideration of the possible time dependent boundary conditions. Solutions can be obtained in a similar way for cylindrical and plate geometries [6]. Here we present results for the cylindrical case. Solving the diffusion equation for a cylindrical geometry without sources:

$$\frac{\partial C}{\partial t} = \frac{\partial}{\partial r}\left(\frac{1}{r} D \partial_r C\right). \tag{1}$$

For the loading phase the initial concentration is assumed to be zero, and a concentration c_L as a boundary condition (with $c_L = K_S\sqrt{p_L}$, p_L the loading pressure) all over the loading time τ:

$$\begin{aligned} &c_1(r, t = 0) = 0 \quad \text{for } 0 < r < a, \\ &c_1(r = a, t) = c_L \quad \text{for } 0 \leqslant t < \tau. \end{aligned} \tag{2}$$

The solution writes as:

$$c_1(r, t) = c_L\left(1 - \frac{2}{a}\sum_{n=1}^{\infty} \frac{1}{\alpha_n} \frac{J_0(r\alpha_n)}{J_1(a\alpha_n)} e^{-D\alpha_n^2 t}\right) \tag{3}$$

with α_n being the roots of $J_0(a\alpha_n)=0$.

For the pumping phase, with a duration Δt, the boundary conditions are expressed as:

$$c_2(r,t=0)=c_1(r,\tau)\quad \text{for } 0<r<a$$
$$c_2(r=a,t)=c_{\mathrm{L}}+\frac{c_{\Delta t}-c_{\mathrm{L}}}{1-\mathrm{e}^{-\beta\,\Delta t}}(1-\mathrm{e}^{-\beta t})\quad \text{for } 0\leqslant t<\Delta t, \tag{4}$$

where $c_{\Delta t}$ is the surface concentration after the pumping time Δt, and β is a free parameter.

These boundary conditions in Eq. (4) have been written assuming:

1. the continuity in time between the final concentration of the loading phase and the initial concentration of the pumping phase: $c_1(a,\tau)=c_{\mathrm{L}}=c_2(a,t=0)$,
2. $c_{\Delta t}$ is defined, i.e. $c_{\Delta t}=c_2(a,\Delta t)$,
3. the decrease of the pressure in the chamber V_1 follows a decreasing exponential curve.

Solutions for $c_2(r,t)$ can be obtained using the superposition theorem (Duhamel's theorem) [7]:

$$c_2(r,t)=\frac{2c_{\mathrm{L}}}{a}\sum_{n=1}^{\infty}\frac{1}{\alpha_n}\frac{J_0(r\alpha_n)}{J_1(a\alpha_n)}\mathrm{e}^{-D\alpha_n^2 t}\left(1-\mathrm{e}^{-D\alpha_n^2\tau}\right)+\frac{2}{a}\sum_{n=1}^{\infty}\frac{1}{\alpha_n}\times\frac{J_0(r\alpha_n)}{J_1(a\alpha_n)}\left(\left(c_{\mathrm{L}}+\frac{c_{\Delta t}-c_{\mathrm{L}}}{1-\mathrm{e}^{-\beta\,\Delta t}}\right)\left(1-\mathrm{e}^{-D\alpha_n^2 t}\right)\right)-\frac{2}{a}\sum_{n=1}^{\infty}D\alpha_n^2\frac{J_0(r\alpha_n)}{J_1(a\alpha_n)}\left(\frac{c_{\Delta t}-c_{\mathrm{L}}}{1-\mathrm{e}^{-\beta\,\Delta t}}\frac{\mathrm{e}^{-\beta t}-\mathrm{e}^{-D\alpha_n^2 t}}{D\alpha_n^2-\beta}\right). \tag{5}$$

For the release phase the boundary conditions can be written as:

$$c_3(r,t=0)=c_2(r,\Delta t)\quad \text{for } 0<r<a,$$
$$c_3(r=a,t)=c_{\Delta t}+\frac{c_f-c_{\Delta t}}{1-\mathrm{e}^{-\gamma\tau}}(1-\mathrm{e}^{-\gamma t})\quad \text{for } 0\leqslant t<\tau. \tag{6}$$

These boundary conditions assume:

1. the continuity between the ending concentration of the pumping phase and the initial concentration of the release phase: $c_2(a,\Delta t)=c_{\Delta t}=c_3(a,t=0)$,
2. the definition of c_f i.e. $c_f=c_3(a,t)$,
3. that the modification of the surface concentration follows the exponential of the pressure increase in the chamber V_1 during the release phase.

The final solution for the concentration distribution in the cylinder during the release phase after the described loading and pumping phases can be written as [6]:

$$c_3(r,t)=\frac{2}{a}\sum_{n=1}^{\infty}\frac{1}{\alpha_n}\frac{J_0(r\alpha_n)}{J_1(a\alpha_n)}\mathrm{e}^{-D\alpha_n^2 t}\Psi_m(\tau,\Delta t)+\frac{2}{a}\sum_{n=1}^{\infty}\frac{1}{\alpha_n}\times\frac{J_0(r\alpha_n)}{J_1(a\alpha_n)}\left(\left(c_{\Delta t}+\frac{c_f-c_{\Delta t}}{1-\mathrm{e}^{-\gamma\,\tau}}\right)\left(1-\mathrm{e}^{-D\alpha_n^2 t}\right)\right)-\frac{2}{a}\sum_{n=1}^{\infty}D\alpha_n^2\frac{J_0(r\alpha_n)}{J_1(a\alpha_n)}\left(\frac{c_f-c_{\Delta t}}{1-\mathrm{e}^{-\gamma\,\tau}}\frac{\mathrm{e}^{-\gamma t}-\mathrm{e}^{-D\alpha_n^2 t}}{D\alpha^2-\gamma}\right), \tag{7}$$

which can be rewritten as:

$$\Psi_m(\tau,\Delta t)=c_{\mathrm{L}}\left(1-\mathrm{e}^{-D\alpha_n^2(\tau+\Delta t)}\right)+\frac{c_{\Delta t}-c_{\mathrm{L}}}{1-\mathrm{e}^{-\beta\,\Delta t}}\left(1-\mathrm{e}^{-D\alpha_n^2\Delta t}-\frac{\mathrm{e}^{-\beta\Delta t}-\mathrm{e}^{-D\alpha_n^2\Delta t}}{D\alpha_n^2-\beta}D\alpha_n^2\right). \tag{8}$$

Once the $c_3(r,t)$ concentration distribution is determined, the hydrogen flux can be explicitly derived:

$$J(t)=-D\nabla c_3(r,t)|_{r=a}. \tag{9}$$

From the time integration of the flux, the total amount of gas in V_1:

$$M(t)=\int_0^t J(t')\,\mathrm{d}t' \tag{10}$$

is derived and expressed in pressure units.

Converting the number of hydrogen atoms to pressure (Pa) in the release volume (V_1-4V_{S}) at temperature T of the chamber V_1 by the factor:

$$\frac{\mathrm{RT}}{(V_1-4V_{\mathrm{S}})2N_{\mathrm{A}}}V_{\mathrm{s}},$$

will finally give the contribution of one cylinder:

$$p(t)=\frac{\mathrm{RT}}{2(V_1-4V_{\mathrm{S}})N_{\mathrm{A}}}V_{\mathrm{s}}\frac{4}{a^2}\sum_{n=1}^{\infty}\frac{1}{\alpha_n^2}\times\left\{\Psi_n(\tau,\Delta t)(1-\mathrm{e}^{-D\alpha_n^2\tau})+A(t)\right\}, \tag{11}$$

with:

$$A(t)=c_{\Delta t}(1-\mathrm{e}^{-D\alpha_n^2\tau})+\frac{c_f-c_{\Delta t}}{1-\mathrm{e}^{-\gamma\tau}}\left(1-\mathrm{e}^{-D\alpha_n^2 t}-\frac{\mathrm{e}^{-\gamma t}-\mathrm{e}^{-D\alpha_n^2 t}}{D\alpha_n^2-\gamma}D\alpha_n^2\right). \tag{12}$$

3.1.1. Free parameters of the model

Our model involves four parameters: D, K_{S}, β, γ. However, the sensitivity of $p(t)$ in Eqs. (11) and (12) to β (and γ) is seen to be low, which could be anticipated from the fact that they appear in temporary boundary conditions. These parameters had been introduced in order to account for possible surface effects (potentially present in open pores of the matrix). In the case of the pure diffusive problem, the input of β (and γ) implies a 2nd order correction to the solution.

The sensitivity of the model to β values is higher than for γ, due to the fact that β enters in the initial concentration for the release phase. The β parameter can be roughly evaluated and related to the gas balance during the pumping phase as:

$$\bar{c}_1(\tau^*) \approx c_L = K_s\sqrt{p_L}$$
$$\bar{c}_2(\Delta t) \approx c_{\Delta t} = c_L(1 - e^{-\beta\,\Delta t}) = K_s\sqrt{p_{\Delta t}}, \quad (13)$$

$$\beta \approx \frac{1}{\Delta t}\sqrt{\frac{p_{\Delta t}}{p_L}} \approx 10^{-5}. \quad (14)$$

This order of magnitude value of β is retained as a reference.

The parameters for which $p(t)$ in Eqs. (11) and (12) shows the highest sensitivity are D and K_s. They are the real free parameters of the model and they are retained hereafter as the main parameters for the modelling of the IDE results.

3.1.2. Validating the model

Commercially available software [8] has been used to implement the model in order to fit the experimental release runs. It has been validated by comparing its predictions for different τ, T and p_L values with the existing literature measurements for nickel (average of 20 measurements) [9], and with the results from the Ni calibration tests of our own facility [10]. About 20 files have been used for the validation, with temperatures ranging from 300 to 800 K, with values of τ as low as 1 h. An example of the quality of the fitting obtained for nickel is shown in Fig. 3. The values of D and K_s derived from such fitting are presented in Figs. 4 and 5 and are compared with existing results in Table 1.

Based on the very good quality of the model predictions for a homogeneous material (Ni), the model was used to obtain tentatively the apparent values for D and K_s for CFCs. However, when it was used to reproduce the hydrogen release profile from CFC, the fitting quality was poor (Fig. 6). The experimental release curve for the three CFC materials studied showed the existence of two different and overlapping time processes during the release history. This suggested that the release curve is composed of a contribution from both fibres and matrix. Nevertheless, the experimental curves can be approached within experimental error bars of ±5%. We use the word apparent (i.e. volume averaged) for the values of D and K_s (±30–40%) derived from these fittings.

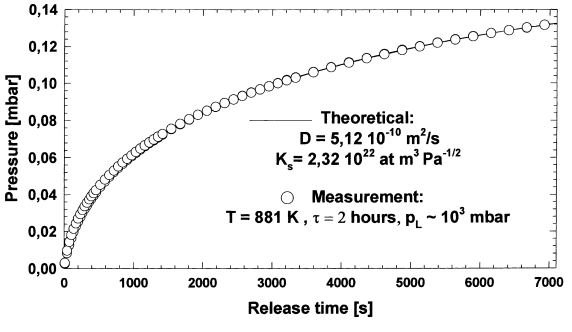

Fig. 3. Fitting the hydrogen release curves from nickel.

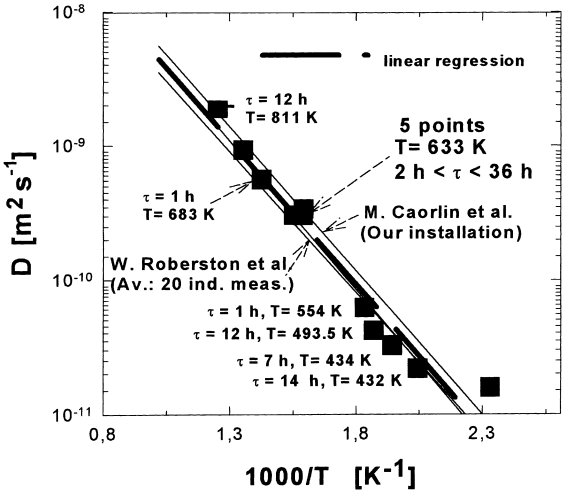

Fig. 4. Values of hydrogen diffusivity in nickel. Test of the model for τ and T.

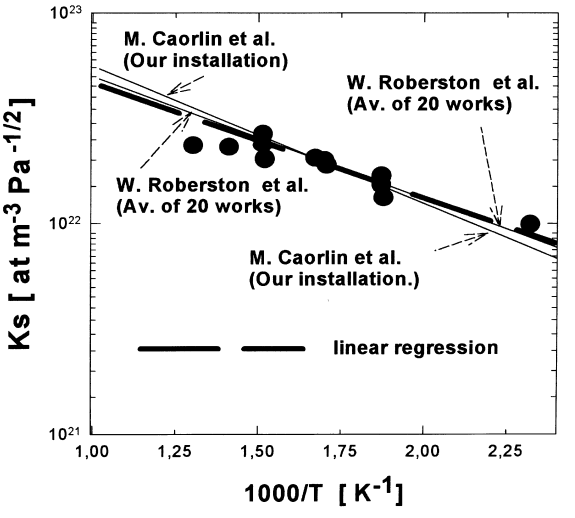

Fig. 5. Values of the Sieverts' constant of hydrogen in Ni. Test of the model for τ and T.

Hence, the satisfactory precision shown by our model developed (Figs. 3–5 and Table 1) enables a drastic reduction in the measuring times to derive apparent hydrogen transport constants for CFCs.

The Arrhenius plots for the apparent values of D and K_s for the three tested CFCs are shown in Figs. 7 and 8, respectively.

4. Hydrogen transport parameters in CFCs

In comparison to Ni, which is a homogeneous material, all of the CFCs tested exhibited a hydrogen

Table 1
Comparison of values obtained for Ni with other existing results

Reference	D_0 (m^2/s)	E_d (kJ/mol)	K_{s0} (at.fr.$Pa^{-1/2}$)	E_s (kJ/mol)
W. Roberston [6]	3.72×10^{-7}	40.20	5.52×10^{-6}	12.5
M. Caorlin [a] [7]	8.63×10^{-7}	41.08	1.87×10^{-6}	8.24
Present work	6.23×10^{-7}	40.91	5.92×10^{-6}	7.96

[a] From the previous calibration of our facility.

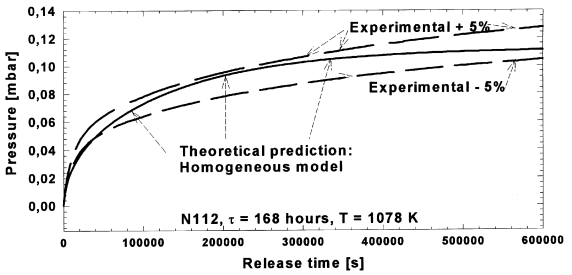

Fig. 6. Fitting quality for CFCs from the homogeneous model.

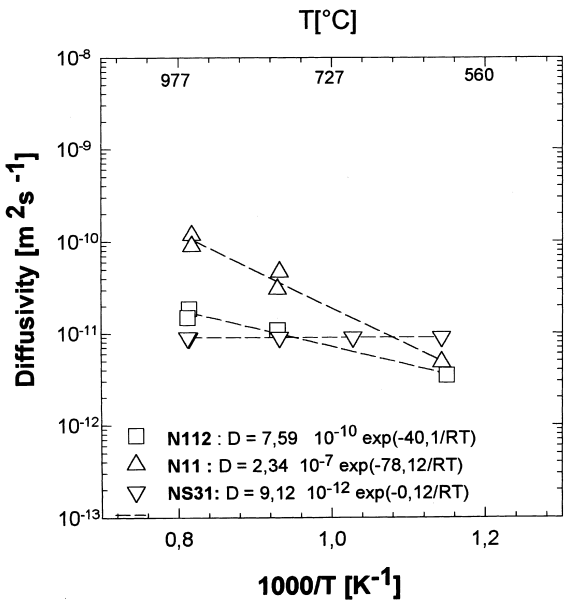

Fig. 7. The apparent diffusivity of hydrogen in three CFC: N112, N11 and NS31 (R: kJ/K mol).

release composed of two overlapping processes. As a consequence of this, the effort to obtain a good fitting of experimental curves and to derive accurate diffusivity and Sieverts constant values for hydrogen was unsuccessful (Fig. 6). This fact provided the driving force for us to elaborate a non-homogeneous model for the study of hydrogen transport in CFC.

It is possible to think in terms of the time constants of the transport processes and of the preferential paths for

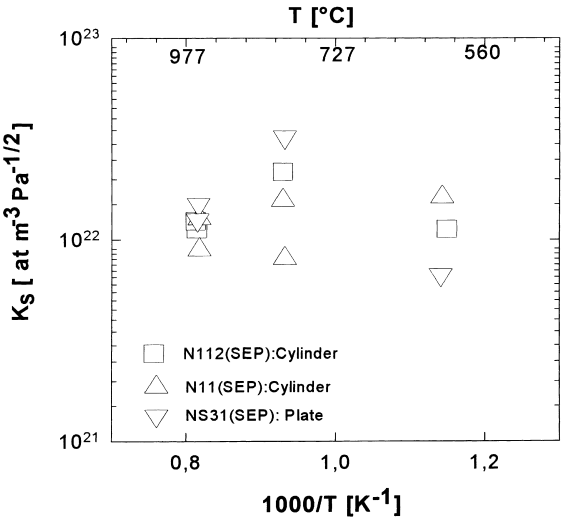

Fig. 8. The apparent Sieverts' constant of hydrogen in three CFC: N112, N11 and NS31.

the hydrogen release (respectively loading) from the composite.

4.1. Radial transport

The ratio between the axial and radial matrix dimensions is about 5%, which as an approximation is possible to consider the samples (hence matrix) as infinitely long cylinders. Due to their dimensions, fibres can be immediately assumed as infinitely long cylinders. Then, the hydrogen transport in each composite's sub-system (fibre F and matrix M) can be postulated as being radial.

4.2. Fibre's role and diffusive time constants

The CFCs studied have fibre distributions as shown in Fig. 9. For drawing clarity, the relative fibre-to-matrix dimensions have been arbitrarily exaggerated.

The general situation for the distribution and radial shapes of diversely distributed fibres within the CFC-matrix has been labelled F1, F2 and F3. The F1-shape corresponds to a vertical, non-centred and non-coaxial to sample fibre, F2 is a vertical and centred coaxial fibre and F3 a general cut of a horizontal fibre.

Under the main hypothesis of radial transport and reversibility of loading to release, it is possible to show as a first-order approximation that, regardless of its position and orientation within the matrix, each fibre should have a similar quantitative contribution to time diffusive constants.

Within the radial and diffusive approximation, the loading of F1 and F2 fibres has an equal (flux-averaged) time- limiting constant (τ):

$$\tau_{F1} \cong \frac{(r-d)^2}{D_M \alpha_0^2}\frac{c_L D_M}{r-d} + \frac{(r+d)^2}{D_M \alpha_0^2}\frac{c_L D_M}{r+d} = \frac{c_L}{\alpha_0^2} 2r$$
$$= \frac{r^2}{D_M \alpha_0^2}\frac{c_L D_M}{r} + \frac{r^2}{D_M \alpha_0^2}\frac{c_L D_M}{r} \cong \tau_{F2}. \quad (15)$$

The same justification is valid for the contribution of any of the points (X-points in Fig. 9) distributed along F3 taking into account that there are no axial gradients along F3. Once the fibres are loaded with hydrogen, the reversibility hypothesis implies that the preceding arguments are also valid for the release phase. Hence, the total fibre contribution can be accounted for by their volumetric fraction, i.e. 1-fibre approximation.

4.3. Hydrogen paths in CFC

Due to the nature of the material (*matrix*: 60 volume% or more depending on each CFC, *fibre*: balanced) [5] a direct contribution to the released flux to V_1 comes from the amount of gas directly loaded in the composite's matrix (M) and subsequently released to V_1: $M \rightarrow V_1$.

Another contribution should come from the amount of gas loaded in the composite's fibres. The amount of hydrogen soluble in the fibre should cross the matrix before contributing to the increase of the pressure in V_1: $F \rightarrow M \rightarrow V_1$.

Other processes potentially present could be:

- $M \rightarrow F \rightarrow M \rightarrow (\ldots) \rightarrow V_1$: Negligible, as a first approximation in comparison to: $M \rightarrow V_1$.

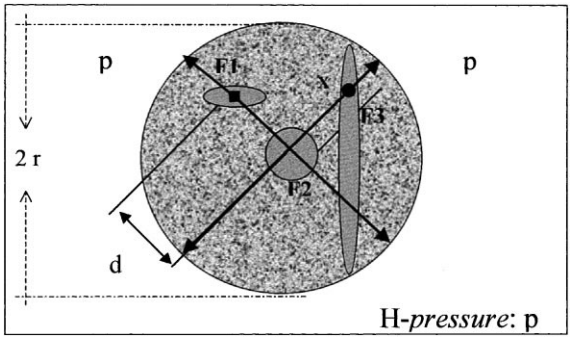

Fig. 9. A general axial cut and radial shapes of divers fibres in the CFC- matrix.

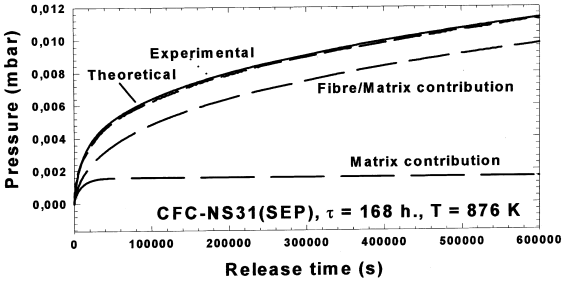

Fig. 10. Fitting quality in CFC from the non-homogeneous transient model.

- $F \rightarrow M \rightarrow F \rightarrow M \rightarrow (\ldots) \rightarrow V_1$: Negligible, in a first approximation in comparison to: $F \rightarrow M \rightarrow V_1$ because the processes works in parallel with the primary processes $M \rightarrow V_1$ and $F \rightarrow M \rightarrow V_1$ and are slower compared to them.

Therefore, at a given temperature, two quantities in parallel should govern the hydrogen kinetics during the loading and release in the composite: $r^2 (D_M \alpha_0^2)^{-1}$ and $r^2 (D_{FM} \alpha_0^2)^{-1}$ for the cylindrical case and $\Delta x^2 (D_M \alpha_0^2)^{-1}$ and $\Delta x^2 (D_{FM} \alpha_0^2)^{-1}$ for the plate case.

At this point we should be able to reproduce the experimental release curve as the addition of two homogeneous-like contributions, keeping in mind that each term includes:

- the matrix constants D_M and $(K_s)_M$,
- the equivalent time constant of a in-series system fibre/matrix and the hydrogen solubility in the fibre $[D_{M-F}, (K_s)_F]$.

An example of the present fitting of the experimental data and their very good quality ($\chi^2 < 10^{-6}$) is shown in Fig. 10. In order to fit the experimental curve, we used two different sets of transport parameters: $[D_M, (K_s)_M]$ and $[(D_{M-F}, (K_s)_F]$, which then enable us to derive the values of D_M, D_{M-F} and D_F. Hence, the intrinsic hydrogen transport values in the CFC sub-systems, fibres and matrix, can be obtained. The diffusivity values are shown in Fig. 11 and the Sieverts constant in Fig. 12.

5. Discussion

As a further checking of the model's quality, the D and K_S values for two N112 specimens with different size (diameters: 6 and 12 mm) are quite similar (Figs. 13 and 14). The slight discrepancies come from a non-negligible axial flux contribution: $\simeq$25% for the case with $\phi = 12$ mm. The apparent values for D and K_s derived for both cases are identical. The hydrogen transport parameters in different CFCs obtained with the above model are coherent and support the assumption of atomic solution of hydrogen in CFC which has been also found by Atsumi et al. [3] in pyrolytic graphite.

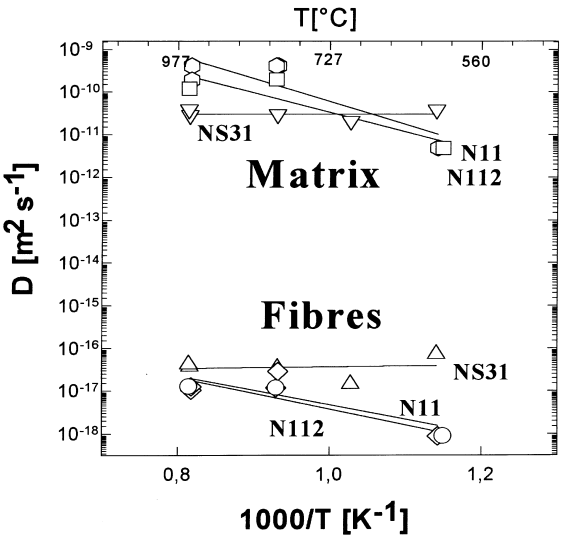

Fig. 11. Intrinsic values for the hydrogen diffusivity in CFC fibre and matrix.

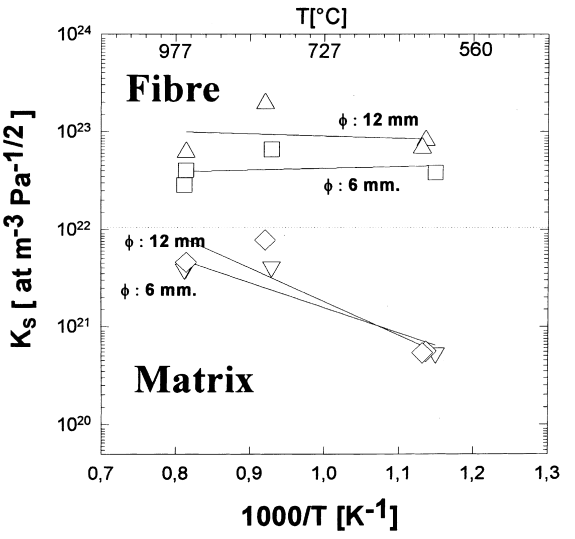

Fig. 13. Intrinsic values for the hydrogen Sieverts' constant in CFC subsystems for two different sized N112 samples.

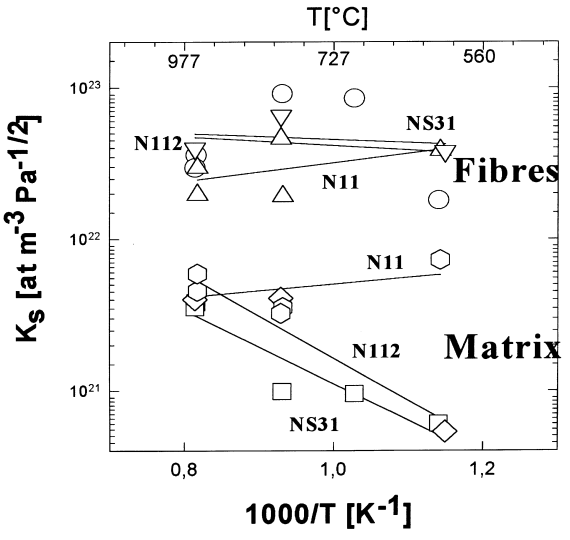

Fig. 12. Intrinsic values for the hydrogen Sieverts' constant in CFC fibre and matrix.

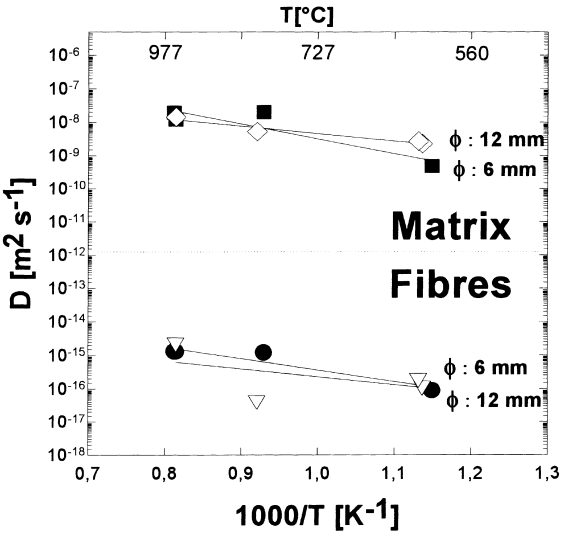

Fig. 14. Intrinsic values for the hydrogen diffusivity in CFC subsystems for two different sized N112 samples.

As far as the apparent diffusivity is concerned, the values obtained are five to seven orders of magnitude larger than those for other types of graphite (IG-110U or G-32), while exhibiting similar E_d. Taking into account the manifest of the Arrhenius dependence of the apparent diffusivity on T (Fig. 7), Knudsen diffusion [11] characterising collisions between molecules and pore walls, with a $T^{-1/2}$ dependence for D, seems to play a negligible role in our measurements.

Regarding the apparent Sieverts' constant (Fig. 8), the knee-trend obtained agrees with those observed for high-density graphite in [12] where two kinds of trapping sites determine the K_s behaviour with a decrease of retention due to the thermal depopulation of the trapping sites. This assessment is coherent with the results in Figs. 12 and 13, where it is shown that a larger bundle-of-fibre subsystem determines the apparent K_s of hydrogen in the CFC.

Fig. 11 shows a gap in the diffusivity pre-exponential factor D_0 in the equation $D = D_0 \exp(-E_d/RT)$ for fibre and matrix suggesting that the same processes govern the hydrogen diffusion in the bulk of both carbon subsystems. Such a gap may be explained assuming a reduction of the mean-free-path of hydrogen in the bulk of the matrix due to the presence of small (5–50 nm) connected pores in the matrix volume.

The exothermal solubility behaviour ($-E_s > 0$) shown by the matrix with the highest porosity (N11) indicates that the porosity should have a complex effect on the total K_s value for the matrix. At the reference test temperatures and loading pressures, hydrogen loads quickly and without significant thermal influence the inner volume of connected pores in the matrix (V_1). The amount of hydrogen confined in such region is completely pumped away during the second phase of the experiment (pumping phase), so it is not available to contribute to the release phase. The high N11 matrix porosity could contribute to c_L by the increase of the hydrogen inlet partial pressure in matrix microcavities, favouring the intake of hydrogen into the bulk matrix. For the relatively low temperatures of our IDE, hydrogen dissolution in pores and/or trapping at the interfaces and other defects aside from pores might have a high importance [12,13] to explain the N11-matrix behaviour.

6. Summary

The good quality and the precision of the non-stationary model developed for IDE for homogeneous metals and non-homogeneous composites are shown. It enables a drastic reduction of measuring time to derive D and K_s for CFCs. The apparent values (i.e. volume averaged) and the intrinsic values for the hydrogen diffusivity in CFC subsystems (fibre and matrix) have been evaluated for three different CFCs. The analysis of the dependence of D and K_s of hydrogen in CFCs, indicates the determinant role of the matrix porosity on the overall diffusivity and the determinant role of fibres on the total solubility. The differentiation of the hydrogen interaction with fibre and matrix will enable to track better hydrogen interaction with the CFC materials. The developed model, in co-ordination with IDE, could be used to support the manufacture of CFC materials, enabling the CFC to be tailored for transport properties, according to their specific technological requirements.

Acknowledgements

The authors wish to thank the Société Européenne de Propulsion (SEP) providing us the samples and additional information needed for these calculations.

References

[1] V. Malka, H.D. Röhrig, R. Hecker, Tritium technology in fission, fusion and isotope application, in: Proceedings of the Conference, Dayton, OH, American Nuclear Society, 1980, p. 102.
[2] K. Ashida, K. Watanabe, J. Nucl. Mater. 183 (1991) 89.
[3] H. Atsumi, S. Tokura, M. Miyake, J. Nucl. Mater. 155–157 (1988) 241.
[4] S. Alberici, A. Perujo, J. Camposilvan, Fusion Technol. 28 (1995) 1108.
[5] SEP. EU-Patents.
[6] L.A. Sedano, CEC Report EUR 17320 EN (1997). CL-NA-17320-EN-C, Printed in Italy.
[7] H.S. Carslaw, J.C. Jaeger, Conduction of Heat in Solids, 2nd ed., OSP, 1959, p. 29.
[8] MATHCAD6.0+. MS4.00 Version. User's Guide.
[9] W.M. Roberston, Z. Metallkund. 64 (1973) 436.
[10] M. Caorlin, J. Camposilvan, F. Reiter, in: Proceedings of the Eighth AIV Nat. Vac. Congress, L' Aquila, Italy, 1983, vol. 2, p. 713.
[11] D.M. Ruthven, Principles of Adsorption and Absorption Processes, Wiley, New York, 1984, p. 123.
[12] G. Federici, C.H. Wu, J. Nucl. Mater. 186 (1992) 131.
[13] R.A. Causey, K.L. Wilson, J. Nucl. Mater. 138 (1986) 57.